ARL-TR-9956 ● AUG 2024

Impact of Proximity Effects on the Magnetic Field Produced by a Multiconductor Cable

by Timothy M Pritchett

NOTICES

Disclaimers

ARL-TR-9956 ● AUG 2024

Impact of Proximity Effects on the Magnetic Field Produced by a Multiconductor Cable

Timothy M Pritchett
DEVCOM Army Research Laboratory

REPORT DOCUMENTATION PAGE

1. REPORT DATE	2. REPORT TYPE	3. DATES COVERED START DATE	END DATE
August 2024	Technical Report	1 Dec 2023	30 June 2024

4. TITLE AND SUBTITLE
Impact of Proximity Effects on the Magnetic Field Produced by a Multiconductor Cable

5a. CONTRACT NUMBER	5b. GRANT NUMBER	5c. PROGRAM ELEMENT NUMBER
5d. PROJECT NUMBER	**5e. TASK NUMBER**	**5f. WORK UNIT NUMBER**
R.0056911.4971		

6. AUTHOR(S)
Timothy M Pritchett

7. PERFORMING ORGANIZATION NAME(S) AND ADDRESS(ES)	8. PERFORMING ORGANIZATION REPORT NUMBER
DEVCOM Army Research Laboratory ATTN: FCDD- RLA-LB Adelphi, MD 20783-1138	ARL-TR-9956

9. SPONSORING/MONITORING AGENCY NAME(S) AND ADDRESS(ES)	10. SPONSOR/MONITOR'S ACRONYM(S)	11. SPONSOR/MONITOR'S REPORT NUMBER(S)
Naval Sea Systems Command 1333 Isaac Hull Ave SE, Bldg. 197 Washington, DC 20376	NAVSEA	

12. DISTRIBUTION/AVAILABILITY STATEMENT
DISTRIBUTION STATEMENT A. Approved for public release: distribution unlimited.

13. SUPPLEMENTARY NOTES
ORCID ID: Timothy M Pritchett, 0000-0002-8024-0850

14. ABSTRACT
We quantify the impact of proximity effects on the magnetic flux density (B-field) due to the current in one of the conductors in a multiconductor cable. Ignoring these effects results in large errors (~40%) in estimates of the magnitude of the field arising from a 1-kHz alternating current, but negligible error (at most, several tenths of a percent) in the magnitude of the field due to currents at power-line frequencies (50–60 Hz). We conclude that ignoring proximity effects in noncontact electric power sensing will not significantly affect the load current estimates obtained from existing US Army Combat Capabilities Development Command Army Research Laboratory methods—except in the case of nonlinear switching loads such as DC power supplies, which can generate significant harmonics in the 1-kHz range.

15. SUBJECT TERMS
proximity effects, multiconductor cable, three-phase cable, magnetic field, noncontact electric power sensing, Electromagnetic Spectrum Sciences

16. SECURITY CLASSIFICATION OF: a. REPORT	b. ABSTRACT	C. THIS PAGE	17. LIMITATION OF ABSTRACT	18. NUMBER OF PAGES
UNCLASSIFIED	UNCLASSIFIED	UNCLASSIFIED	UU	40

19a. NAME OF RESPONSIBLE PERSON	19b. PHONE NUMBER *(Include area code)*
Timothy M Pritchett	(301) 394-0332

STANDARD FORM 298 (REV. 5/2020)
Prescribed by ANSI Std. Z39.18

Contents

List of Figures

Executive Summary

Methods developed by the US Army Combat Capabilities Development Command Army Research Laboratory for noncontact electric power sensing assume that the magnetic field produced by a conductor in a multiconductor cable is not significantly affected by currents in the other conductors.[*] Strictly speaking, this is only true for DC and/or for filamentary conductors. The field produced by time-varying currents in the other conductors gives rise to a redistribution of current density within the conductor in question, and this redistribution is reflected in an alteration in the field produced by that conductor. The literature on these "proximity effects" is extensive. This work leverages published results[†] to quantify the error introduced by the presence of additional conductors carrying currents of comparable amplitude.

We find that a second conductor carrying 1-kHz AC induces a relative error of up to 40% in the field produced by a nearby conductor carrying 1-kHz AC of comparable amplitude. At a frequency of 50 Hz, however, the relative error in field magnitude is less than 0.5%. If the current carried by the second conductor is significantly greater than that carried by the conductor in question, the relative error in the magnitude of the field produced by the latter is correspondingly greater. However, in this case, the overall magnetic field measured by sensors outside the cable is dominated by the contribution from the second conductor.

The published results employed in this study were obtained for an idealized system—a pair of infinitely long, straight, parallel, cylindrical wires carrying equal and opposite currents—that differs in many respects from a three-phase power cable with twisted conductors. Nonetheless, we believe that the overall conclusion of this study remains valid in the case of the cable: namely, that at AC power frequencies (50–60 Hz), the magnetic field arising from the current flowing in a conductor suffers only a negligible relative perturbation from currents in nearby conductors, provided all currents are of roughly comparable amplitude.

An exact numerical solution of the three-phase twisted cable problem would require a modest extension of our codebase. The components of the complex (phasor) vector potential $\vec{A}$ satisfy an inhomogeneous Helmholtz equation within the conductors and the Laplace equation in the region outside the conductors. We possess a solver for the latter partial differential equation (PDE), and a solution of

[*] Claytor KE, Hull DM, inventors; US Department of Army, assignee. Non-contact power meter independent of placement of field sensors around cable. United States patent US 11,566,918. 2023 Jan 31.

† Coufal O. Current density in two parallel cylindrical conductors and their inductance. Electr Eng. 2017;99:519–523.

the former can be constructed from the solution of the associated homogeneous Helmholtz equation, for which we also possess a working solver. After known problems with our existing domain decomposition method (DDM) solver have been corrected, we could leverage its methods to match the solutions in the various regions, as the boundary conditions on $\vec{A}$ and its normal derivative on the surfaces of the conductors are very similar to those enforced on the scalar potential and its derivatives on the boundaries of neighboring domains in the DDM.

1. Introduction

The US Army Combat Capabilities Development Command (DEVCOM) Army Research Laboratory (ARL) has developed a mobile power meter (MPM) for nonintrusive monitoring of power systems.[1] The MPM employs noncontact electric and magnetic field sensors at multiple locations around a three-phase power cable. Because the sensors are positioned outside the insulated power cable, the device can be safely installed in less than a minute without the need for a disruptive power outage or a skilled electrician. The field measurements obtained from the MPM are converted into estimates of the voltages and currents associated with each of the three conductors in the cable using methods also developed at ARL.

Noncontact power system monitoring relies on the accuracy with which information about charge distributions and currents (i.e., "sources") can be derived from information about the electric and magnetic fields that they produce in a region of space. Inverse problems such as this abound in science and engineering, and they can in general be very difficult to solve.

Recent laboratory trials revealed unacceptably large errors in the values of the voltages and currents predicted by the ARL algorithm in certain cases. For this reason, we reexamine the various approximations and simplifying assumptions that underlie our methods.

The magnetic field outside a multiconductor cable is the superposition of the fields arising from the currents carried by each of the individual conductors in the cable. ARL methods represent the field configuration outside the three-phase power cable as a linear combination of three single-conductor "basis functions," each of which is given by the field configuration produced when one of the conductors carries unit current and the remaining conductors carry zero current; the expansion coefficients are then simply the estimated currents in each conductor. The model makes the tacit assumption that the single-conductor basis functions are constant, that is, that the field configuration arising from a unit current in one conductor does not change in the presence of nonvanishing currents in one or both of the other conductors. Unfortunately, this is simply not the case. To be sure, the *total current* carried by the conductor in question is unaffected by the fields produced by currents in the other conductors. However, those fields give rise to a shift in the *distribution of current density* within the given conductor, and this redistribution is reflected in an alteration in the field produced by that conductor. These "proximity effects" are well documented in the literature.[2–7] The same mechanism gives rise to the skin effect, an identical redistribution of current density within a single conductor.[3,4,6]

The magnetic proximity effects present in a multiconductor cable find an electrostatic analog in a system of perfectly conducting, charged spheres. In the case of a single sphere bearing total charge Q, the charge distributes itself uniformly over the surface of the sphere, and the electric field outside the sphere is simply the spherically symmetric field of a point charge Q. If a second sphere bearing the identical charge Q is now placed next to the first, the charge on each sphere redistributes itself to an equilibrium configuration in which there is relatively low surface charge density in the region of each sphere that is nearest the other sphere, and relatively high surface charge density in the antipodal region that is farthest from the other sphere. The combined electric field of the pair of charged spheres is no longer that of a pair of identical point charges Q, as would be the case if the charge on each sphere were frozen in place and unable to move in response to the electrostatic repulsion from the charge on the other sphere.

In the same way as the charge on the surface of a conducting sphere redistributes itself in response to the electric field arising from charge on other spheres, so too does the current density over the cross section of a conductor redistribute itself in response to the magnetic field arising from currents in the nearby conductors. The latter interaction is the result of Faraday's law, so it is possible that for sinusoidal currents and fields at AC power frequencies the single-conductor magnetic field configurations that form the basis functions in the ARL model can indeed be taken to be constant to a good approximation. However, this assumption must be verified. We do so here. In this work, we leverage published results[2] to quantify the error in our model introduced by the presence of additional conductors carrying currents of comparable amplitude.

2. Magnetic Flux Density of an Infinitely Long, Straight, Cylindrical Wire Carrying an Arbitrary Current Density

As illustrated in Fig. 1, an infinitely long, straight, cylindrical wire of radius a and coaxial with the z-axis carries a current density $J(\rho, \varphi)\,\hat{z}$ that is *not* necessarily symmetric about the axis. In this section, we derive an expression for the magnetic flux density $\vec{B}(\rho, \varphi)$ in the region outside the wire. Here and throughout this report we employ Gaussian units except where otherwise indicated.

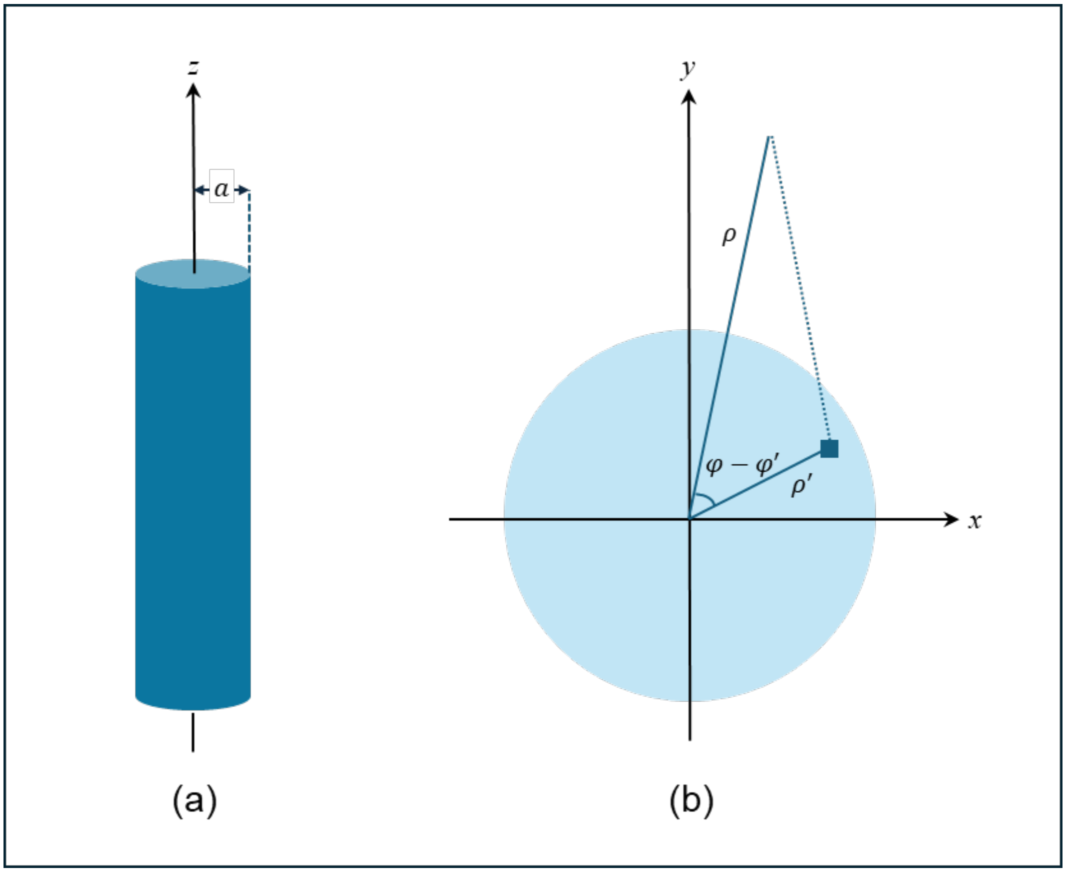

Fig. 1 **(a) Geometry of the problem: an infinitely long, straight, cylindrical wire. (b) Cross section of the wire showing the coordinates used in the integration over the current density. The *z*-axis is directed out of the page.**

The problem is most easily approached via the vector potential $\vec{A}(\vec{x})$, which is related to the magnetic flux density $\vec{B}(\vec{x})$ by

$$\vec{B}(\vec{x}) = \vec{\nabla} \times \vec{A}(\vec{x}) \, . \tag{1}$$

The components of the vector potential in the *xy*-plane vanish, and the *z*-component may be obtained by integrating the contributions from the currents in infinitesimal filaments over the cross section of the wire:

$$dA_z(\rho, \varphi) = -\frac{2}{c} \ln(|\rho\hat{\rho} - \rho'\hat{\rho}'|) \; J(\rho', \varphi') \, \rho' d\rho' d\varphi' \, . \tag{2}$$

The argument of the natural logarithm on the right-hand side of Eq. 2 is the perpendicular distance between the filament and the point at which the vector potential is being evaluated. It is represented in Fig. 1b by the dotted line and may be obtained from the law of cosines. The resulting expression may be expanded in an infinite series,[8] which for $\rho' < \rho$ takes the form given in the second equality below:

$$\ln(|\rho\hat{\rho} - \rho'\hat{\rho}'|) = \ln\left(\left[\rho^2 + {\rho'}^2 - 2\rho\rho'\cos(\varphi - \varphi')\right]^{1/2}\right)$$
$$= \ln(\rho) - \sum_{m=1}^{\infty} \frac{1}{m}\left(\frac{\rho'}{\rho}\right)^m \cos[m(\varphi - \varphi')]\,. \tag{3}$$

Integrating over the cross section of the cylindrical wire, we obtain

$$A_z(\rho,\varphi) = -\frac{2I}{c}\ln(\rho) + \frac{2}{c}\sum_{m=1}^{\infty}\frac{1}{m}\int_0^a d\rho'\rho'\left(\frac{\rho'}{\rho}\right)^m \int_{-\pi}^{\pi} d\varphi'\, J(\rho',\varphi')\cos[m(\varphi-\varphi')]\,, \tag{4}$$

where I is the total current carried by the wire:

$$I = \int_0^a d\rho'\rho' \int_{-\pi}^{\pi} d\varphi'\, J(\rho',\varphi'). \tag{5}$$

Equation 4 is ideal for analytic calculations like those in the next section but ill-suited for cases in which the integration must be performed numerically. For this reason, we introduce the integrals $\mathcal{C}_m$ and $\mathcal{S}_m$, defined

$$\begin{bmatrix}\mathcal{C}_m\\ \mathcal{S}_m\end{bmatrix} = \int_0^a du\, u^{m+1}\int_{-\pi}^{\pi} dv\, J(u,v)\begin{bmatrix}\cos(mv)\\ \sin(mv)\end{bmatrix}, \tag{6}$$

and we use them to rewrite Eq. 4 as

$$A_z(\rho,\varphi) = -\frac{2I}{c}\ln(\rho) + \frac{2}{c}\sum_{m=1}^{\infty}\frac{\rho^{-m}}{m}\{\mathcal{C}_m\cos(m\varphi) + \mathcal{S}_m\sin(m\varphi)\}. \tag{7}$$

Finally, we compute the curl of $\vec{A}(\rho,\varphi)$ to obtain the magnetic flux density:

$$\vec{B}(\rho,\varphi) = \frac{2I}{c\rho}\hat{\varphi} + \frac{2}{c}\sum_{m=1}^{\infty}\frac{1}{\rho^{m+1}}\{\mathcal{C}_m[-\sin(m\varphi)\,\hat{\rho} + \cos(m\varphi)\,\hat{\varphi}] + \mathcal{S}_m[\ \ \cos(m\varphi)\,\hat{\rho} + \sin(m\varphi)\,\hat{\varphi}]\}\,. \tag{8}$$

Returning to Eq. 6, we observe that if the current density is axially symmetric (i.e., $J(u,v) = J(u)$, independent of the angular variable v), then the angular integrals vanish for all values of m and the expression for $\vec{B}(\rho)$ reduces to a single term,

$$\vec{B}_0(\rho) = \frac{2I}{c\rho}\hat{\varphi}\,, \tag{9}$$

the familiar expression for the magnetic flux density outside an infinitely long, straight wire carrying total current I. We denote this field configuration by $\vec{B}_0$. We emphasize that the result in Eq. 9 applies only if the distribution of current over the cross section of the wire is axially symmetric, but it applies to *all* such axially symmetric distributions of current.

3. An Illustrative Example: *B*-field Arising from a Current Density Distribution Without Axial Symmetry

A magnetic field inherits the symmetries—or lack thereof—of the currents that produce it. To best highlight the implications of this, we begin with an illustrative example. In this section, we examine the magnetic flux density $\vec{B}(\rho, \varphi)$ outside the cylindrical conductor shown in Fig. 1 that results from a representative current density $\vec{J}(\rho, \varphi)$ that lacks axial symmetry and may be expressed analytically:

$$\vec{J}(\varphi) = J_0 \cos(\varphi/2)\, \hat{z}\,. \tag{10}$$

Here, $J_0 = I/[2a^2]$, where I is the total current carried by the wire, given by Eq. 5. The distribution of current density over the cross section of the wire is shown in Fig. 2.

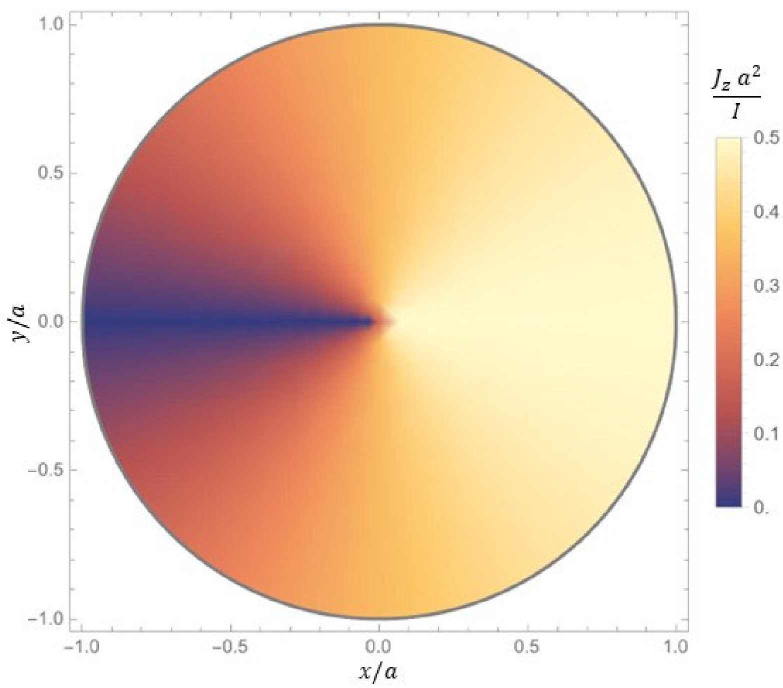

Fig. 2 Non-axially symmetric current density $\vec{J}(\varphi) = J_0 \cos(\varphi/2)\, \hat{z}$ in a cylindrical wire of radius a carrying total current I. Here $J_0 = I/[2a^2]$ and the unit vector $\hat{z}$ is directed along the wire (out of the page in the figure).

In this example, $J(\varphi)$ is symmetric about the *x*-axis: $J(\varphi) = J(-\varphi)$, so the integrals $\mathcal{S}_m$ vanish for all values of m, and the expression for $\vec{B}(\rho, \varphi)$ in Eq. 8 reduces to

$$\vec{B}(\rho, \varphi) = \frac{2I}{c\rho}\hat{\varphi} + \frac{4I}{ca}\sum_{m=1}^{\infty} \frac{(-1)^m}{(4m^2-1)(m+2)} \left(\frac{a}{\rho}\right)^{m+1} [\sin(m\varphi)\, \hat{\rho} - \cos(m\varphi)\, \hat{\varphi}]. \tag{11}$$

Figure 3 shows the vector field $\vec{B}$ outside a 1-cm-diameter wire carrying a total current of 1 A (2.998×10^9 esu/s) distributed over the cylindrical cross section of the wire per Eq. 10. The magnitude in gauss of the magnetic flux density outside the conductor is indicated by the color scale, which is the same for both panels of the figure, and the direction of the field is indicated by the arrows. (In Fig. 3, the field lines indicate only the direction of the field; the magnitude is indicated exclusively by the color scale.) The upper panel, Fig. 3a, depicts the field that arises from an arbitrary axially symmetric distribution of current density in the wire; that field is given by Eq. 9. The lower panel, Fig. 3b, displays the field resulting from the current density distribution given by Eq. 10 and shown in Fig. 2, which lacks axial symmetry. A comparison of the two panels reveals that the absence of axial symmetry results in a field that is not directed tangentially.

Of course, Ampère's law has not been suspended; in particular, the integral formulation of Ampère's law,

$$\oint_C \vec{B} \cdot d\vec{\ell} = \frac{4\pi}{c} \iint_S \vec{J} \cdot \hat{n}\, dA = \frac{4\pi}{c} I_{\text{enclosed}} \,, \tag{12}$$

continues to hold for any closed curve C and for any surface S having C as its boundary. This means that as long as C completely encircles the wire, the total current enclosed by C, I_{enclosed}, must be 1 A, regardless of how the current is distributed over the cross section of the wire. We verified that this is true for the two field configurations shown in Fig. 3, as well as for all field configurations presented below (for which we will take the total current I carried by the wire to be 1 A).

Figure 4 helps to explain what is going on. As we have seen, a deviation from axial symmetry in $\vec{J}(\rho, \varphi)$ manifests itself as a discrepancy $\Delta\vec{B}(\rho, \varphi)$ between the resulting field $\vec{B}(\rho, \varphi)$, which is given by Eq. 8, and the axially symmetric field $\vec{B}_0(\rho)$, given by Eq. 9:

$$\Delta\vec{B}(\rho, \varphi) = \vec{B}(\rho, \varphi) - \vec{B}_0(\rho) \,. \tag{13}$$

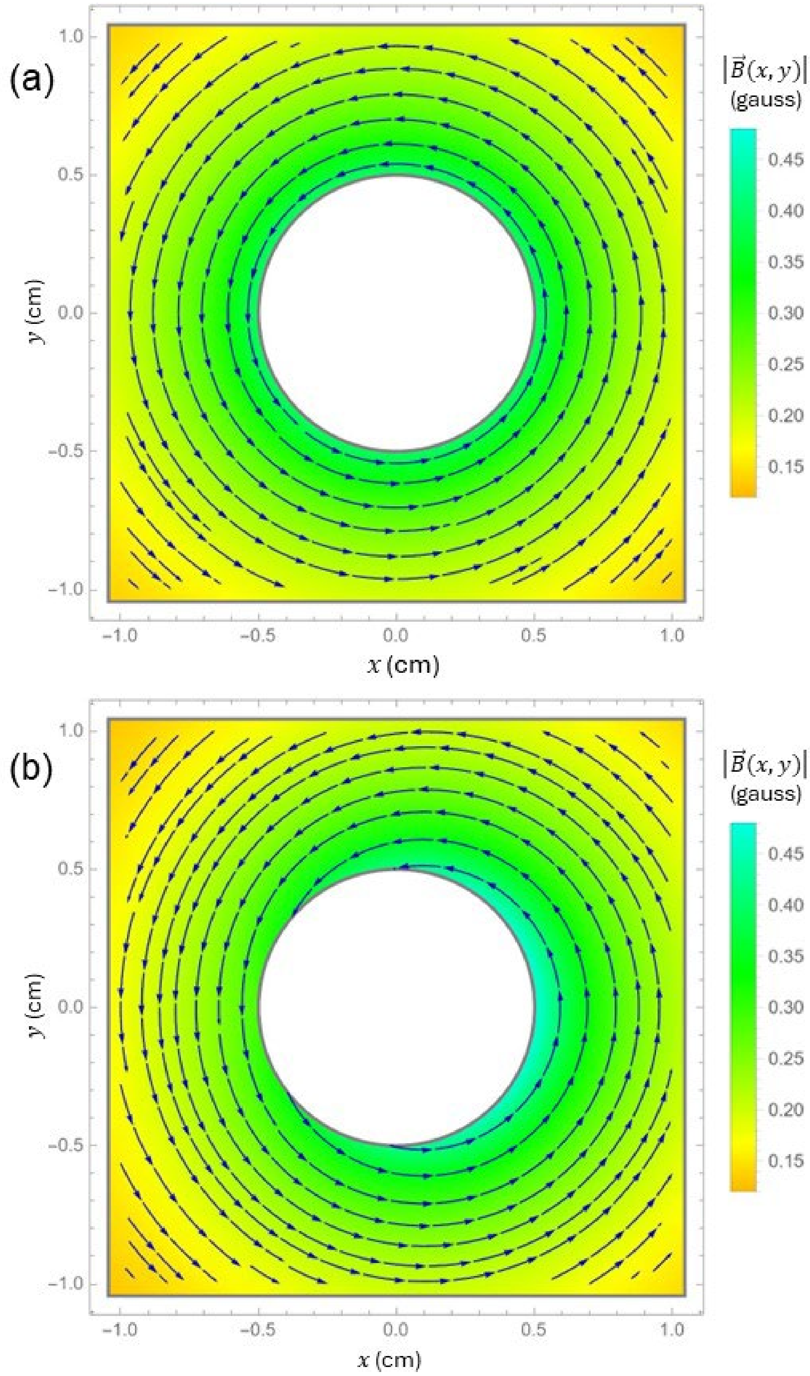

Fig. 3 **Magnetic flux density $\vec{B}(x,y)$ outside a wire of radius $a = 0.5$ cm carrying a 1-A current directed out of the page. The magnitude in gauss of the field in each panel is indicated by the common color scale on the right. (a) *B*-field resulting from an axially symmetric current density delivering a total current of 1 A. (b) *B*-field produced by the current density $\vec{J}(\varphi) = \hat{z}\,(1\text{ A})\cos(\varphi/2)/[2a^2]$, which also delivers a total current of 1 A but lacks axial symmetry.**

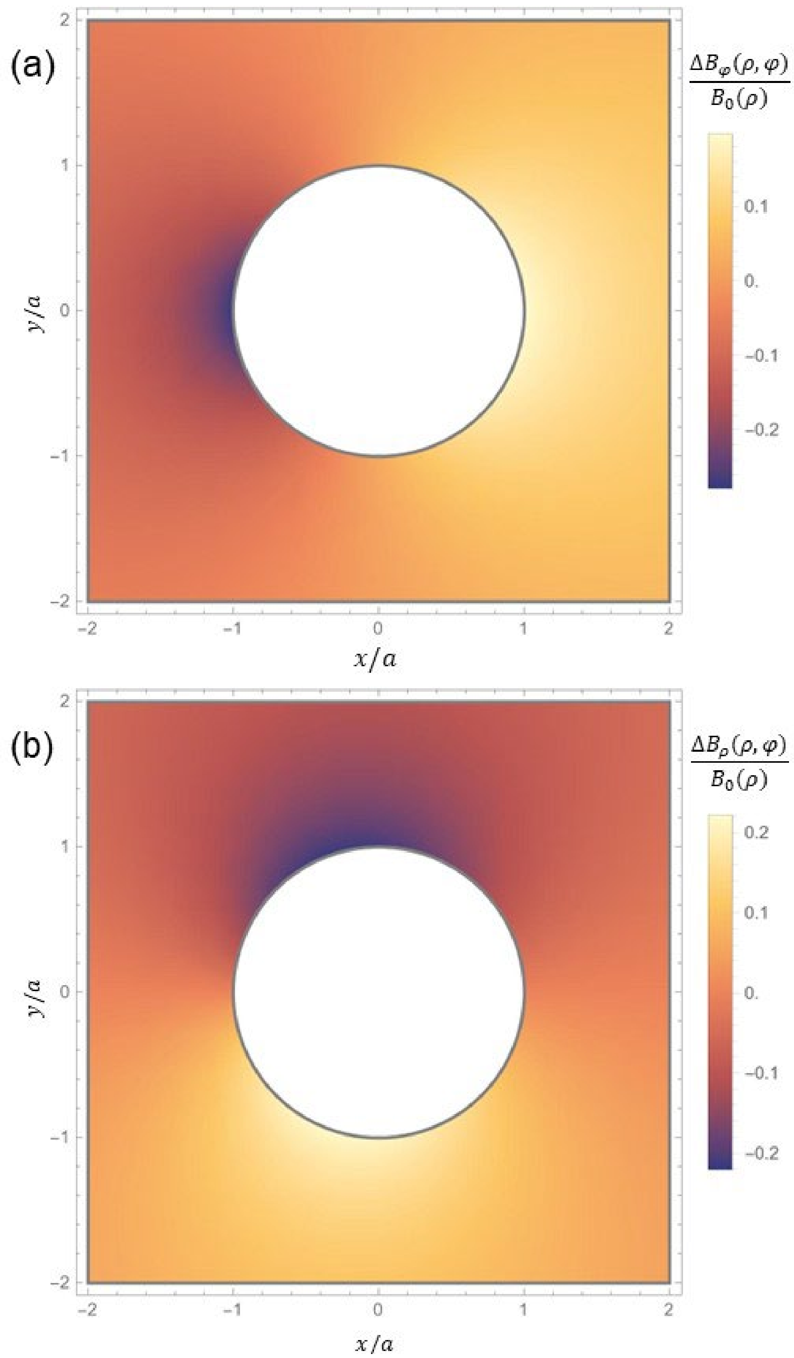

Fig. 4 **Relative discrepancy $\Delta\vec{B}(\rho,\varphi)/B_0(\rho)$ in magnetic flux density due to the absence of axial symmetry in the distribution of current density over the cross section of a cylindrical wire of radius a carrying total current I. The discrepancy is relative to the field $\vec{B}_0(\rho) = 2I\hat{\varphi}/[c\rho]$ produced by a current density that is axially symmetric over the cross section of the wire. It is normalized by $B_0(\rho)$ at each point. The current density within the wire is given by $\vec{J}(\varphi) = \hat{z}\,(1\text{ A})\cos(\varphi/2)/[2a^2]$. (a) Relative discrepancy $\Delta B_\varphi(\rho,\varphi)/B_0(\rho)$ in the tangential component of the field. (b) Relative discrepancy $\Delta B_\rho(\rho,\varphi)/B_0(\rho)$ in the radial component of the field.**

The discrepancy is given by the infinite sum that appears on the right-hand side of Eq. 8, and its tangential and radial components, normalized at each point by $B_0(\rho)$, are shown in Figs. 4a and 4b, respectively. For *any* closed path C encircling the wire,

$$\oint_C \Delta\vec{B} \cdot d\vec{\ell} = 0 , \tag{14}$$

so a positive discrepancy in some region of C must be compensated for by negative discrepancies elsewhere on the curve. Figure 4 makes it plausible how this might occur.

Finally, in Fig. 5 we plot the percentage error in $|\vec{B}(\rho,\varphi)|$ relative to the axially symmetric field given by Eq. 9.

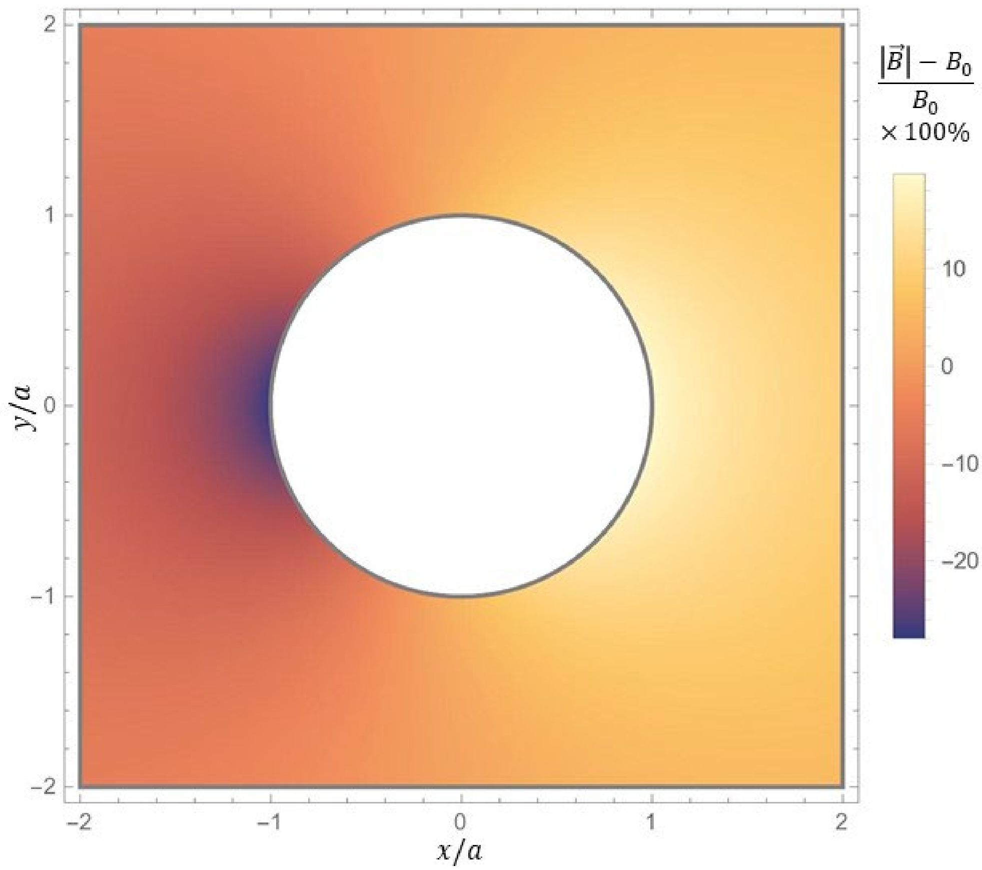

Fig. 5 Percent error in the magnitude $|\vec{B}|$ of the field arising from the current density $\vec{J}(\varphi) = J_0 \cos(\varphi/2)\,\hat{z}$, which is not axially symmetric, relative to the field magnitude $B_0(\rho) = 2I/[c\rho]$ arising from an axially symmetric current density distribution delivering the same total current I.

4. Magnetic Flux Density Resulting from the Current Density Arising from Proximity Effects in an Infinite "Lamp Cord"

In his 2017 paper,[2] Coufal models the distribution of current density in the infinite "lamp cord" system illustrated in Fig. 6. The lamp cord consists of a pair of identical, infinitely long, cylindrical copper conductors of radius 5 mm carrying equal and opposite currents directed parallel to the z-axis (left-hand wire in the figure) and antiparallel to the z-axis (right-hand wire). The center-to-center separation of the two wires is set to its limiting value, 10 mm, that is, the thickness of the insulation between the conductors is assumed to be negligible.

As Fig. 6 shows, the lamp cord system is invariant under the operation of reflection in the xz-plane. The distribution of current density over the cross section of each conductor, shown in Fig 6b, is thus symmetric about the x-axis, or equivalently: $J(\rho, \varphi) = J(\rho, -\varphi)$. The reader might recall that the current density considered in Section 3 possesses the same symmetry.

Finally, we observe that the lamp cord is also invariant under the (commutative) combined operations of reflection in the plane $x = a$ and reversal of the direction of one of the currents.

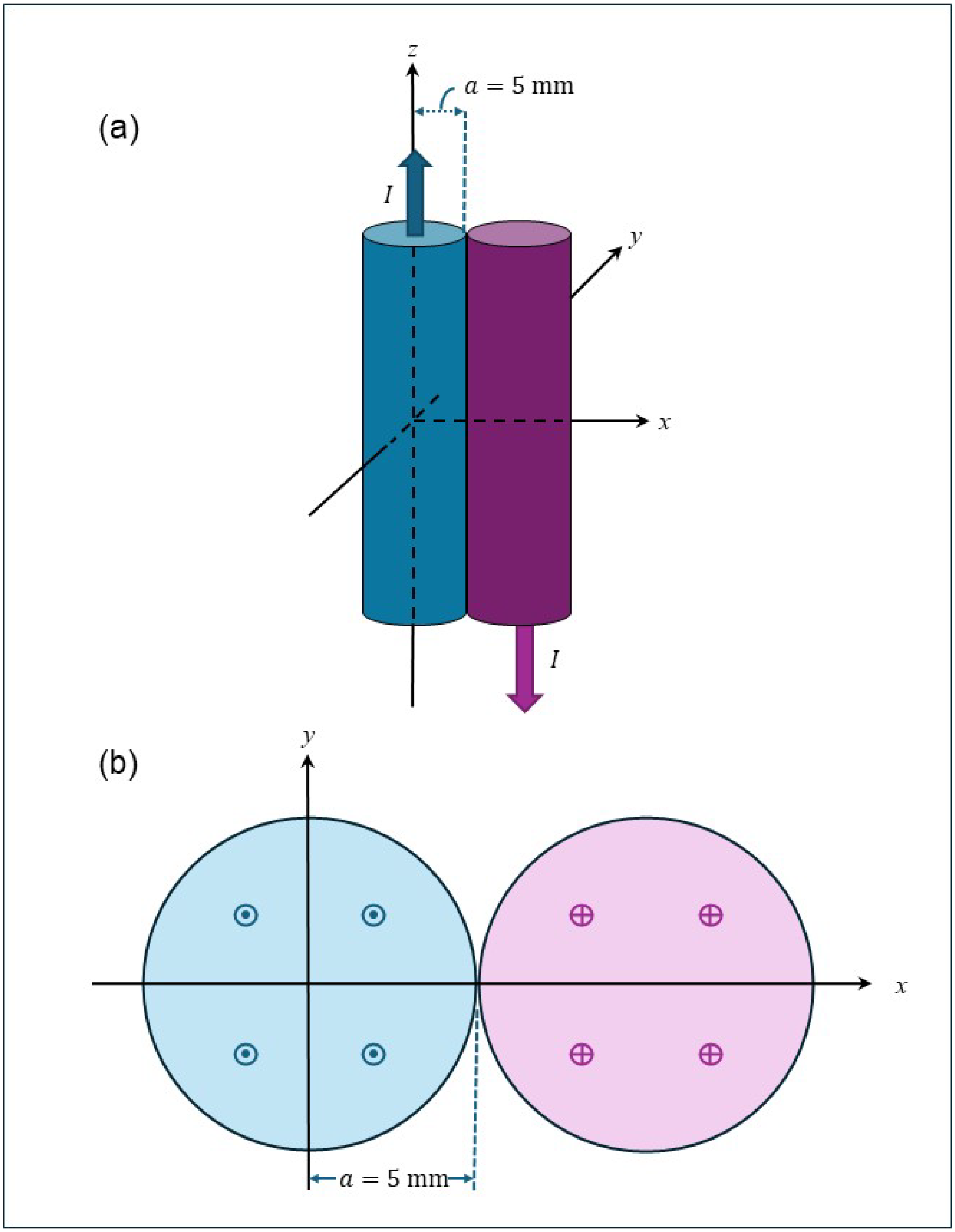

Fig. 6 (a) Geometry of the "lamp cord" system considered in Coufal[2]: a pair of infinitely long, straight, cylindrical wires carrying equal and opposite currents directed parallel and antiparallel to the *z*-axis. (b) Cross section of the two wires showing the coordinates used in Fig. 7 to describe the current density in the left-hand conductor. The *z*-axis is directed out of the page.

4.1 *B*-field Due to the Current Density Reported in Coufal 2017 for 1-kHz Alternating Current

The current density within an individual conductor in a multiconductor AC power cable is the vector sum of an “applied” current density (i.e., the current density in the conductor absent inductive effects) and an “induced” current density arising from the time-varying magnetic field produced by currents in other conductors. Coufal’s calculation accounts for the effect of the induced current on the current density within the conductors.[2]

The contour plot reproduced in Fig. 7a, which appears as Fig. 3 in Coufal,[2] displays the current density $\vec{J}(x,y) = J(x,y)\,\hat{z}$ in the upper half of the cross section of the left-hand conductor of the infinite lamp cord system carrying 1-kHz AC. (The current density is symmetric about the x-axis in Fig. 7, so only the upper half of the cross section is shown.) The contour plot was captured using WebDigitizer and intermediate values of the normalized current density were estimated using linear interpolation. Figure 7b displays the results. In both Figs. 7a and 7b, $\vec{J}(x,y)$ is normalized by $J_0 = I/[21.2\ \mathrm{mm}^2]$, where I is the total current carried by the wire.

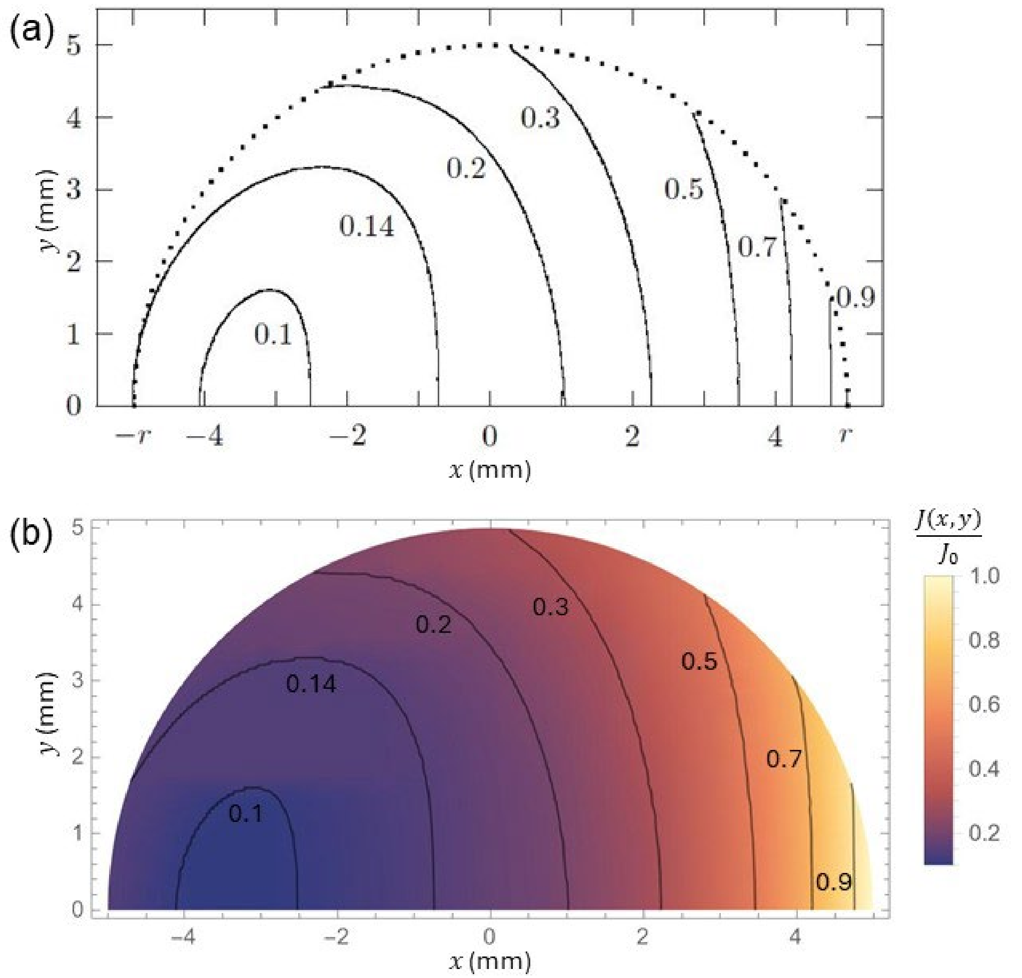

Fig. 7 Normalized current density $J(x, y)\,\hat{z}\,/\,J_0$ in the upper half of the cross section of the left-hand conductor of the infinite lamp cord shown in Fig. 6 carrying 1-kHz AC. Here, $J_0 = I/[21.2\ \mathrm{mm}^2]$, where I is the total current carried by the wire. (a) Contour plot of computational results, published as Fig. 3 in Coufal.[2] (b) Normalized current density profile employed in the calculations in this report; $J(x, y)$ is a continuous function for which the values on the contour lines match those in Fig. 7a and intermediate values are estimated by linear interpolation in the plane.

The current density $J(x, y)$ plotted in Fig. 7b was re-expressed as a function $J(\rho, \varphi)$ of the polar coordinates ρ and φ and inserted into Eq. 6. Because $J(\rho, \varphi)$ is an even function of the angular variable: $J(\rho, \varphi) = J(\rho, -\varphi)$, the integrals $\mathcal{S}_m$ vanish identically for all values of m. The integrals $\mathcal{C}_m$ were computed numerically, and $\vec{B}(\rho, \varphi)$ was calculated from Eq. 8, with the sum on the right-hand side truncated after eight terms. Figure 8 shows the resulting vector field $\vec{B}$ outside the left-hand wire of the lamp cord and due only to the current in that conductor; the wire carries a total current of 1 A distributed over the cylindrical cross section as shown in Fig. 7b. The magnitude in gauss of the field is indicated by the color scale, and the direction of the field is indicated by the arrows.

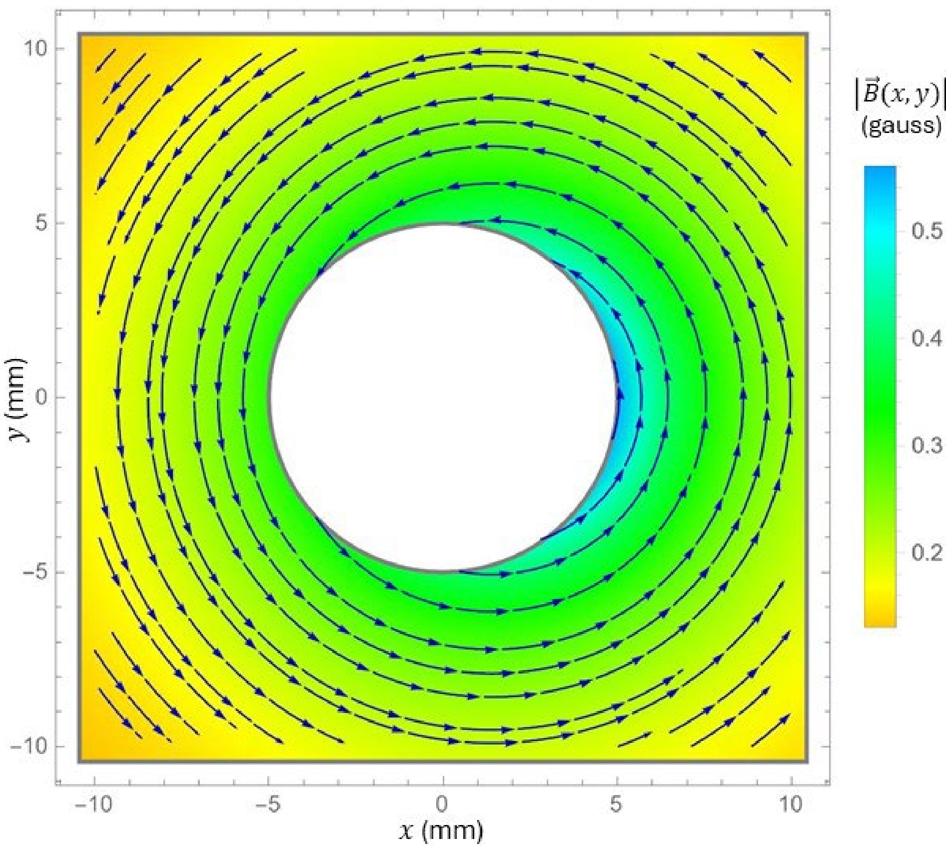

Fig. 8 Vector field $\vec{B}(x,y)$ outside a wire of radius 5 mm carrying a 1-A current directed out of the page. The magnitude in gauss of the field at each point is indicated by the superimposed color map. The field arises from the current density shown in Fig. 7b.

Figures 9a and 9b, respectively, show the tangential and radial components of the discrepancy $\Delta\vec{B}(\rho,\varphi) = \vec{B}(\rho,\varphi) - \vec{B}_0(\rho)$, normalized by the magnitude $B_0(\rho)$ of the axially symmetric field given by Eq. 9. Figure 10 plots the percentage error in $\left|\vec{B}(\rho,\varphi)\right|$ relative to $B_0(\rho)$.

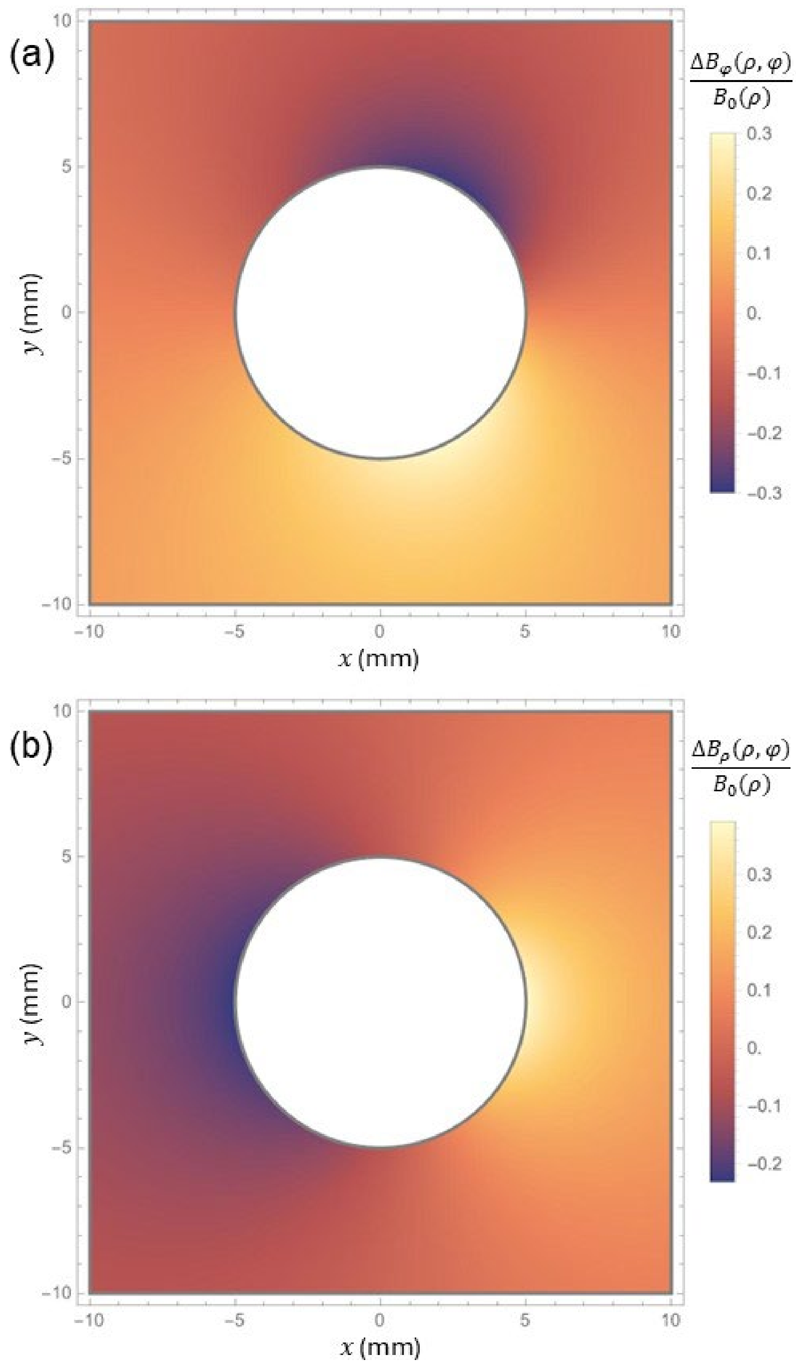

Fig. 9 Relative discrepancy $\Delta\vec{B}(\rho,\varphi)/B_0(\rho)$ in magnetic flux density due to the absence of axial symmetry in the current density reported in Coufal[2] for 1-kHz AC carried by a cylindrical wire of 5-mm radius. The discrepancy is normalized at each point by $B_0(\rho) = 2I/[c\rho]$, the magnitude of the field outside the wire resulting from an arbitrary axially symmetric current density delivering the same total current I. (a) Relative discrepancy $\Delta B_\varphi(\rho,\varphi)/B_0(\rho)$ in the tangential component of the field. (b) Relative discrepancy $\Delta B_\rho(\rho,\varphi)/B_0(\rho)$ in the radial component of the field.

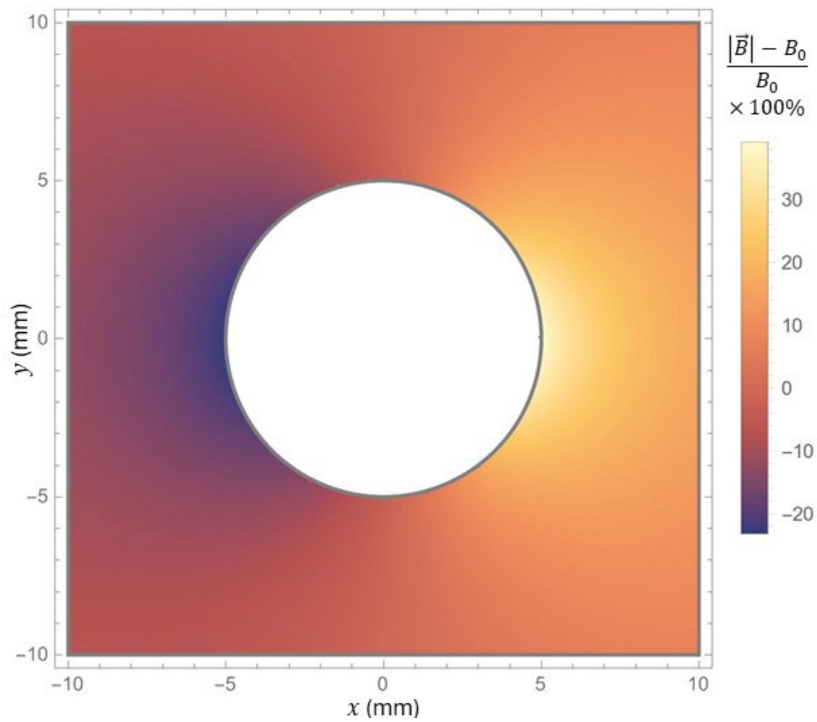

Fig. 10 Percent error in the magnitude $|\vec{B}|$ of the field arising from the current density reported in Coufal[2] for 1-kHz AC, a current density distribution that lacks axial symmetry, relative to the field magnitude $B_0(\rho) = 2I/[c\rho]$ arising from an axially symmetric current density distribution delivering the same total current I.

Legacy ARL methods for noncontact electric power sensing ignore magnetic proximity effects. In the present case of a long, straight conductor carrying current I, they assume that the B-field due to that current is *always* that given by Eq. 9, whatever the currents in neighboring conductors. However, we find that a nearby conductor carrying 1-kHz AC induces a relative error of up to approximately 40% in the magnitude of field produced by a given conductor carrying 1-kHz AC of comparable amplitude. Even though these results apply to frequencies that are 16 to 20 times greater than typical AC power frequencies, they still have implications for our methods. Impulsive currents associated with DC power supplies and other nonlinear switching loads can result in significant load currents at harmonic frequencies in the 1-kHz range. (Indeed, IEEE Standards 1159-2019 and 519-2022 recommend measuring power signals up to the 50th harmonic or more—3 kHz for a 60-Hz power system—for precisely this reason.[9,10]) The error in the field resulting from these high-frequency currents is potentially problematic, as is the associated error in the estimated total harmonic distortion (THD).

4.2 *B*-field Due to a 50-Hz Alternating Current Density Distribution Derived from Reported Results

Coufal does not report the distribution of current density $J(\rho, \varphi)$ over the cross section of a conductor in the infinite lamp cord system at AC power frequencies; he merely observes that at a frequency of 50 Hz, the minimum magnitude of the amplitude of current density in the conductor cross section equals 95.4% of its maximum.[2]

To arrive at an approximate, preliminary conclusion regarding the error due to proximity effects in the magnetic flux density arising from 50-Hz AC, we proceed by simply rescaling the results displayed in Fig. 7b for 1-kHz AC such that the minimum value of the normalized current density $J(\rho, \varphi)/J_0$ over the cross section of the conductor is equal to 0.954, the reported minimum for 50-Hz AC.[2] The resulting rescaled current density distribution is shown in Fig. 11.

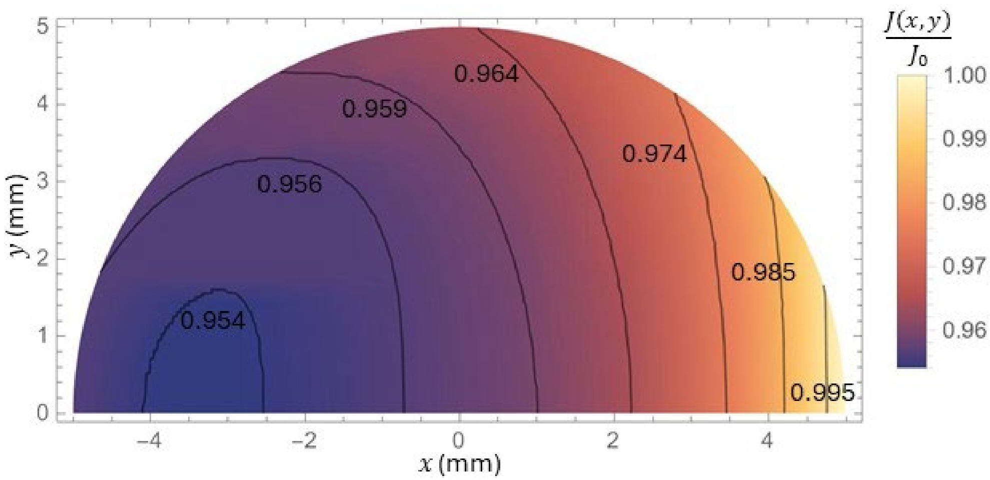

Fig. 11 Normalized current density $\boldsymbol{J(x, y)\,\hat{z}\,/\,J_0}$ for 1-kHz AC from Fig. 7b, rescaled to the level reported in Coufal[2] for 50-Hz AC. Here, $\boldsymbol{J_0 = I/[75.61\ \mathrm{mm}^2]}$, where $\boldsymbol{I}$ is the total current carried by the wire.

The actual current density distribution for 50-Hz AC would be expected to exhibit a greater level of axial symmetry than the distribution shown in Fig. 11. The minimum would be expected to lie closer to the origin, the arcs forming the contour lines to be more circular, and so on. As a result, the level of asymmetry present in the B-field computed from the current density in Fig. 11 would be expected to exceed that of the actual field, and the resulting relative error in $|\vec{B}|$ to represent an upper bound to the relative error in the magnitude of the actual field. Calculations bear these expectations out. The integrals $\mathcal{C}_m$, defined in Eq. 6, were computed numerically from the current density in Fig. 11. As before, the integrals $\mathcal{S}_m$ vanish because of the symmetry of the charge density about the x-axis. The resulting B-field for 50-Hz AC, computed using Eq. 8, is shown in Fig. 12a. For ease of comparison, the corresponding the B-field for 1-kHz AC, depicted in Fig. 8, is reproduced in Fig. 12b.

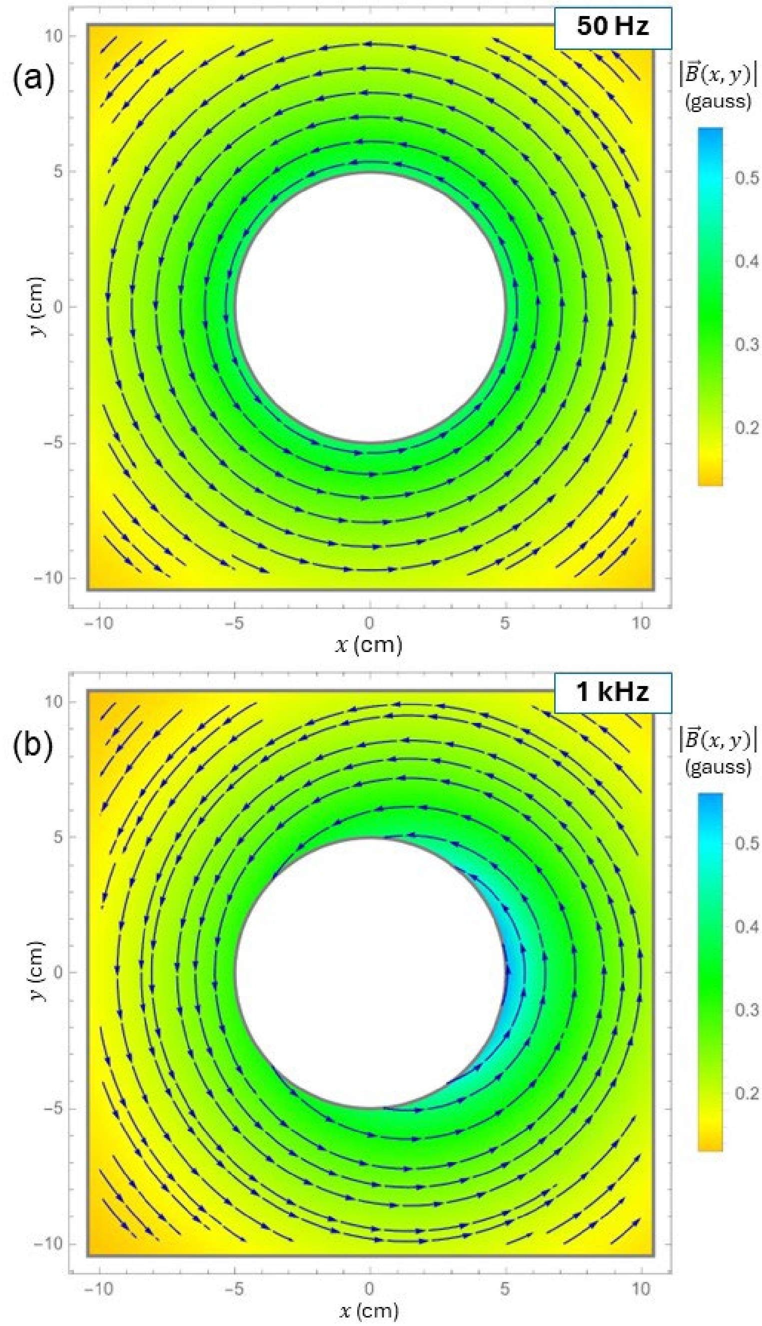

Fig. 12 Vector field $\vec{B}(x, y)$ outside a wire of radius 5 mm carrying a 1-A current directed out of the page, superimposed on a color map giving the magnitude in gauss of the field at each point. Both plots use the same color scale. (a) Field arising from the estimated current density for 50-Hz AC, shown in Fig. 11. (b) Field arising from the current density reported in Coufal[2] for a 1-kHz AC.

The vector field in Fig. 12a, which arises from 50-Hz AC, displays visibly more cylindrical symmetry than the 1-kHz AC field in Fig 12b. This is reflected in the values of the percentage error in $|\vec{B}(x,y)|$, which are some two orders of magnitude lower for the former field; compare the color scales in the legends in Figs. 10 and 13.

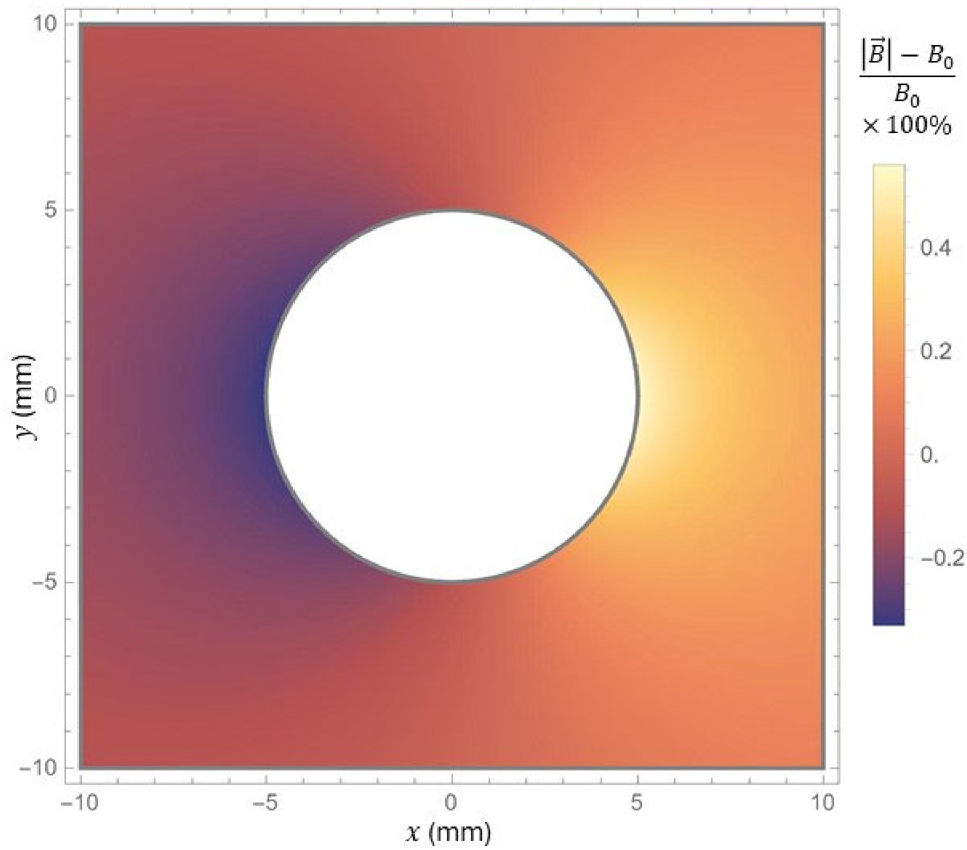

Fig. 13 Percent error in the magnitude of the field arising from the current density derived from Fig. 3 in Coufal[2] and rescaled to the level reported for a 50-Hz alternating current, relative to the field magnitude $B_0(\rho) = 2I/[c\rho]$ arising from an axially symmetric current density distribution delivering the same total current I. The percent error shown represents an upper bound to the percent error in the actual field.

4.3 Discussion

The published results employed in this study were obtained for an idealized system—a pair of infinitely long, straight, parallel, cylindrical wires carrying equal and opposite currents—that differs in many respects from a three-phase twisted power cable. Moreover, the current density distribution for 50-Hz AC was not calculated from first principles; it was merely estimated from results reported for 1-kHz AC.[2] Nonetheless, we believe that the overall conclusion of this study remains valid in the case of the three-phase cable: namely, that at AC power frequencies, the magnetic field arising from the current flowing in a conductor suffers only a negligible relative perturbation from currents in nearby conductors, provided all currents are of roughly comparable amplitude.

Based on these preliminary results, the 50–60-Hz fields obtained from the magnetic model employed in ARL noncontact power sensing methods are expected to exhibit less than 0.5% error relative to the measured fields. However, fields at harmonic frequencies (up to 3 kHz) and/or vehicular auxiliary power units running at 400 Hz may have more significant errors, possibly exceeding 10%.

In Section 5, we discuss how we might remedy the deficiencies noted above.

5. Toward an Exact Solution for a Three-Phase Twisted Cable

With very few exceptions, reports in the literature of magnetic field proximity effects in multiconductor systems are limited to studies involving long, straight conductors, which may even be treated analytically. Notably, Machado et al. apply analytic methods to straight, three-conductor bundles of overhead power transmission lines,[4] and Brito et al. do the same for straight, three-phase underground power cables.[6] Clearly, however, the problem of calculating the magnetic field arising from the twisted conductors that compose a three-phase twisted power cable will have to be treated numerically. In this section, we discuss the relevant PDEs and specify the associated boundary value problem.

5.1 Vector Potential Inside and Around a Conductor Carrying Current

We consider a collection of conducting wires carrying sinusoidal currents of angular frequency ω. We denote the magnetic permeability and electric conductivity of a given wire by μ and σ, respectively. These quantities, as well as the phase of the current, may have different values in different wires. The components of the vector potential $\vec{A}(\vec{x})$ are complex (phasor) quantities. In the interior of a conductor, $\vec{A}(\vec{x})$ satisfies an inhomogeneous Helmholtz equation, and in the dielectric medium surrounding the conductors, the Laplace equation.

$$\nabla^2 \vec{A}(\vec{x}) = \begin{cases} \frac{4\pi\sigma\mu}{c^2}\left[i\omega\vec{A}(\vec{x}) - c\vec{\eta}(\vec{x})\right], & \text{inside conductors} \\ 0, & \text{in the dielectric outside conductors} \end{cases} \tag{15}$$

Here, $\vec{\eta}(\vec{x}) = -\hat{s}(\vec{x})\ dV/ds$ is the voltage drop per unit length of the wire in question, directed along the axis of the wire. Equation 15 follows from Maxwell's equations, Ohm's law, and the constitutive relation between the magnetic flux density $\vec{B}$ and the magnetic field strength $\vec{H}$. The Appendix contains a derivation of this result and additional discussion.

It is straightforward to construct a solution $\vec{A}_{in}(\vec{x})$ of the inhomogeneous Helmholtz equation (Eq. 15 with right-hand side given by the upper expression in the brace) from a solution $\vec{A}_0(\vec{x})$ of the associated homogeneous Helmholtz equation. Let $\vec{A}_0(\vec{x})$ be a solution of

$$[\nabla^2 + k^2]\,\vec{A}_0(\vec{x}) = 0\,, \tag{16}$$

where $k = e^{-i\pi/4}\,\sqrt{4\pi\sigma\mu\omega}\,/\,c$. The vector potential inside a given conductor is then

$$\vec{A}_{in}(\vec{x}) = \vec{A}_0(\vec{x}) - i\frac{c}{\omega}\vec{\eta}(\vec{x})\,. \tag{17}$$

Thus, we need only solve the homogenous equation, Eq. 16. We already possess numerical solvers for this equation as well as for the Laplace equation (Eq. 15 with right-hand side given by the lower expression the brace: 0). We discuss the numerical solution of these PDEs in Section 5.3.

5.2 Boundary Conditions

The boundary conditions that $\vec{B}$ and $\vec{H}$ must satisfy at the interface between different media follow from Maxwell's equations and are well known: the component of $\vec{B}$ normal to the interface is continuous across it, as is, in the absence of a surface current density, the tangential component of $\vec{H}$. Expressed in terms of the vector potential $\vec{A}$, the condition on the normal component of $\vec{B}$ is

$$\hat{n}(\vec{x})\cdot\vec{\nabla}\times\left[\vec{A}_{out}(\vec{x}^+) - \vec{A}_{in}(\vec{x}^-)\right] = 0\,, \tag{18}$$

where $\hat{n}(\vec{x})$ is the outward normal to the interface. For the condition given by Eq. 18 to be satisfied, it is sufficient that tangential component of $\vec{A}(\vec{x})$ be continuous across the interface:

$$\hat{n}(\vec{x})\times\left[\vec{A}_{out}(\vec{x}^+) - \vec{A}_{in}(\vec{x}^-)\right] = 0\,. \tag{19}$$

To understand why this is true, consider a point $\vec{x}_0$ on the surface of one of the conducting wires (which is not necessarily straight). One can construct an orthonormal coordinate system at $\vec{x}_0$ with unit vectors $\hat{n}(\vec{x}_0)$, the outward normal to the surface of the wire; $\hat{s}(\vec{x}_0)$, a unit vector in the direction of the wire; and $\hat{t}(\vec{x}_0) \stackrel{\text{def}}{=} \hat{s}(\vec{x}_0)\times\hat{n}(\vec{x}_0)$. In the event that the wire is straight and coaxial with the *z*-axis, the vectors $\hat{n}(\vec{x}_0)$, $\hat{t}(\vec{x}_0)$, and $\hat{s}(\vec{x}_0)$ reduce, respectively, to $\hat{\rho}$, $\hat{\varphi}$, and $\hat{z}$, the familiar unit vectors in a cylindrical coordinate system.

The tangent plane to the wire at $\vec{x}_0$ is spanned by $\hat{s}(\vec{x}_0)$ and $\hat{\tau}(\vec{x}_0)$. The normal component of the curl in Eq. 18 acts only on the components of $\vec{A}$ that are tangential to the interface (the s- and τ-components in our orthonormal system), and it only contains derivatives with respect to coordinates in the tangent plane (s and τ in our system). Thus, if the tangential components of $\vec{A}$ are continuous across the interface, then their derivatives in directions tangent to the interface must necessarily be continuous as well.

The condition on the tangential component of $\vec{H}$ is

$$\hat{n}(\vec{x}) \times \vec{\nabla} \times \left[\frac{\vec{A}_{out}(\vec{x}^{+})}{\mu_{out}} - \frac{\vec{A}_{in}(\vec{x}^{-})}{\mu_{in}}\right] = 0 \,, \tag{20}$$

where $\mu_{out} = 1$ and $\mu_{in} = \mu$.

We intentionally express the boundary conditions in Eqs. 19 and 20 in the most general possible way to facilitate their use in treating a twisted cable via a numerical solution procedure. In the case of a straight wire (no twist), there is considerable simplification: only the component of $\vec{A}$ parallel to the wire (*z*-component) is non-zero, and the boundary conditions, expressed in a cylindrical coordinate system with *z*-axis coaxial with the wire, simplify to

$$A_{z\,out}(\vec{x}^{+}) = A_{z\,in}(\vec{x}^{-}) \tag{21}$$

$$\frac{1}{\mu_{out}} \frac{\partial A_{z\,out}}{\partial \rho}\bigg|_{\vec{x}^{+}} = \frac{1}{\mu_{in}} \frac{\partial A_{z\,in}}{\partial \rho}\bigg|_{\vec{x}^{-}} . \tag{22}$$

5.3 Numerical Solution

We have already observed that the geometric complexity introduced by the twist leaves us little choice but to employ numerical methods in our efforts to compute the magnetic field of a three-phase twisted power cable. Fortunately, many of the individual pieces of software necessary to implement such a solution already exist in our codebase.

- For each conductor, our existing Helmholtz solver can be used to obtain the solution $\vec{A}_0(\vec{x})$ to the homogenous Helmholtz equation specified by Eq. 16. From $\vec{A}_0(\vec{x})$, we construct $\vec{A}_{in}(\vec{x})$, the solution for the vector potential inside the conductor, per Eq. 17.
- Our existing Laplace solver provides the solution $\vec{A}_{out}(\vec{x})$ for the vector potential in the dielectric region outside the conductors.
- Equations 19 and 20, respectively, specify the boundary conditions that components of the vector potential and their derivatives must satisfy on the

surface of the conductors. These are enforced via an iterative procedure in which the preceding two steps are performed repeatedly until the boundary conditions are satisfied.

The third element of this solution procedure is not yet implemented, but its development is already fairly advanced. After known problems with our existing DDM solver have been corrected, we should be able to leverage its methods to match the solutions in the various regions, as the boundary conditions on $\vec{A}$ and its normal derivative on the surfaces of the conductors are very similar to those enforced on the scalar potential and its derivatives on the boundaries of neighboring domains in the DDM.

6. Conclusions

ARL methods for noncontact electric power sensing incorrectly assume that the contribution to the magnetic field arising from current flowing in one of the conductors in a multiconductor power cable is independent of the currents in the other conductors. Laboratory trials have revealed unacceptably large errors (>10%) in the values of the load currents predicted by the ARL algorithm in certain cases. We wanted to determine whether the level of error introduced by the methods' faulty assumption regarding the magnetic field could account for the large errors observed in the trials, or whether it is negligible, and the source of the observed experimental error in the load currents lies elsewhere.

To answer this question as efficiently as possible, we leveraged published results on the distribution of current density within a conductor in a multiconductor system. Redistribution of current density within such a conductor, in response to the field produced by the currents in the other conductors, results in an alteration in the field produced by the conductor in question. This alteration is the error introduced by the faulty assumption made in ARL methods.

Based on results reported by Coufal for a two-conductor system,[2] we found that when proximity effects are accounted for, the magnitude of the B-field due to one of the conductors differs by up to 40% from the magnitude of the field assumed in ARL methods, which ignore proximity effects. This result applies to the case where both conductors carry 1-kHz AC of comparable amplitude. For electric power systems, it thus impacts only the higher harmonics that can be generated by certain nonlinear switching loads. At fundamental frequencies (50–60 Hz), the discrepancy in these magnitudes lies below a few tenths of a percent. Despite the differences between a three-phase twisted power cable and the idealized two-conductor system on which these results are based, we believe that the overall conclusion of this study remains valid in the case of the cable. At AC power frequencies, the magnetic field arising from the current flowing in a conductor suffers only a negligible relative perturbation from currents in nearby conductors, provided all currents are of roughly comparable amplitude.

Resistive loads, which give rise to little or no current at harmonic frequencies, are preferred for use with the legacy ARL methods for noncontact power sensing. In view of this, we must conclude that the failure of these methods to account for proximity effects will have negligible impact on their load current estimates, and the source of the errors observed in laboratory trials must be due to other aspects of the physical experiments not accounted for in the magnetic field model and/or to other deficiencies in the algorithm. Examples of the former include:

- Bend in the cable. The magnetic field model assumes that the cable is straight. The magnitude and direction of the field produced by a bent cable will differ slightly from that produced by a straight cable, although the difference is expected to be minor, provided the bend in the cable is not extreme. More importantly, the conductor-to-sensor distances for an MPM positioned on a bent cable may differ significantly, in relative terms, from those employed in the ARL model.

- Differences and/or variations in the position and twist of conductors relative to their nominal values.

- Proximity to other power cables or to ferromagnetic (steel) and/or highly conducting (aluminum) bulkheads.

The legacy magnetic field model could be extended to account for all the effects enumerated above. Of course, the results would apply only to fundamental electric power frequencies (50–60 Hz), and the error arising from proximity effects at the higher-frequency harmonics generated by certain nonlinear loads would remain.

This report also describes how we could obtain an exact numerical solution to the three-phase twisted cable problem, including proximity effects, with only modest additions to our codebase. The results presented here effectively rule out proximity effects as a significant contributor to the large errors in load current estimates observed in laboratory trials, so such an effort would do little to advance our immediate goal of improving our existing methods to eliminate the observed errors. It would, however, enable us to explore several relevant questions, for example, the way in which the error produced by ignoring proximity effects scales with frequency. In addition, after experimental verification of the error at higher frequencies (>1 kHz), it could also lead to correction factors being added to fields measured at higher harmonics for our THD calculations.

7. References

1. Claytor KE, Hull DM, inventors; US Department of Army, assignee. Non-contact power meter independent of placement of field sensors around cable. United States patent US 11,566,918. 2023 Jan 31.

2. Coufal O. Current density in two parallel cylindrical conductors and their inductance. Electr Eng. 2017;99:519–523.

3. Coufal O. Current density in a long solitary tubular conductor. J Phys A: Math Theor. 2008;41:145401.

4. Machado VM, Pedro ME, Faria JAB, Van Dommelen D. Magnetic field analysis of three-conductor bundles in flat and triangular configurations with the inclusion of proximity and skin effects. Electric Power Syst Res. 2011;81:2005–2014.

5. Coufal O. Current density in two solid parallel conductors and their impedance. Electr Eng. 2014;96:287–297.

6. Brito AI, Machado VM, Almeida ME, Neves MG. Skin and proximity effects in the series-impedance of three-phase underground cables. Electric Power Syst Res. 2016;130:132–138.

7. Coufal O. Current density in a group of long parallel conductors. Phys Scr. 2019;94:125504.

8. Jackson JD. Classical electrodynamics. 2nd ed. John Wiley and Sons; 1975. p. 118, eq. (3.152).

9. IEEE 1159-2019. IEEE recommended practice for monitoring electric power quality. IEEE Power and Energy Society; 2019.

10. IEEE 519-2022. IEEE recommended practice for harmonic control in electric power systems. IEEE Power and Energy Society; 2022.

Appendix. Partial Differential Equations for the Vector Potential Inside a Multiconductor Power Cable and in the Surrounding Region

A.1 Relation Between the Time-dependent Electric Field and the Scalar and Vector Potentials

We generalize the well-known relation between a static or quasi-static electric field $\vec{E}(\vec{x})$ and the scalar potential $\Phi(\vec{x})$,

$$\vec{E}(\vec{x}) = -\vec{\nabla}\Phi(\vec{x}) \ , \qquad \text{(A-1)}$$

to account for time-dependent processes. Our point of departure is Faraday's law:

$$\vec{\nabla} \times \vec{E}(\vec{x},t) + \frac{1}{c}\frac{\partial \vec{B}(\vec{x},t)}{\partial t} = 0 \ . \qquad \text{(A-2)}$$

Substituting $\vec{\nabla} \times \vec{A}(\vec{x})$ for $\vec{B}(\vec{x},t)$ from Eq. 1 and reversing the order of the spatial and temporal derivatives, we obtain

$$\vec{\nabla} \times \left[\vec{E}(\vec{x},t) + \frac{1}{c}\frac{\partial \vec{A}(\vec{x},t)}{\partial t}\right] = 0 \ . \qquad \text{(A-3)}$$

The curl of the gradient of a function vanishes, so Eq. A-3 is satisfied if the quantity in square brackets is the gradient of some scalar function; we identify that function with $-\Phi(\vec{x},t)$, where $\Phi(\vec{x},t)$ is the scalar potential. In this way, we obtain the following relation between the time-dependent electric field and the scalar and vector potentials:

$$\vec{E}(\vec{x},t) = -\vec{\nabla}\Phi(\vec{x},t) - \frac{1}{c}\frac{\partial \vec{A}(\vec{x},t)}{\partial t} \ . \qquad \text{(A-4)}$$

A.2 Vector Potential Inside a Conductor Carrying Current

A collection of conducting wires carries sinusoidal currents of angular frequency ω. The magnetic permeability and electric conductivity of a given wire are μ and σ, respectively. These quantities, as well as the phase of the current, may have different values in different wires.

In the context of a conducting wire, it is useful to think of the first term on the right-hand side of Eq. A-4 as the "applied" electric field, and the second as the "induced" field. The applied field is simply the voltage drop $\vec{\eta}$ per unit length of conductor:

$$\vec{\eta}(\vec{x},t) = -\vec{\nabla}\Phi(\vec{x},t) = -\frac{dV}{ds}\hat{s}(\vec{x}) \ , \qquad \text{(A-5)}$$

where s is arc length along the wire and $\hat{s}(\vec{x})$ is a unit vector in the local direction of the wire; for a straight wire parallel to the z-axis, $\hat{s} = \hat{z}$.

The current density $\vec{J}(\vec{x},t)$ inside a particular wire is given by Ohm's law:

$$\vec{J}(\vec{x},t) = \sigma\,\vec{E}(\vec{x},t) = \sigma\left(\vec{\eta}(\vec{x},t) - \frac{1}{c}\frac{\partial \vec{A}(\vec{x},t)}{\partial t}\right), \tag{A-6}$$

where the second equality follows from Eqs. A-4 and A-5. $\vec{J}(\vec{x},t)$ is related to the magnetic field $\vec{H}(\vec{x},t)$ by Ampère's law:

$$\vec{\nabla} \times \vec{H}(\vec{x},t) = \frac{4\pi}{c}\,\vec{J}(\vec{x},t) + \frac{1}{c}\frac{\partial \vec{D}(\vec{x},t)}{\partial t}\,. \tag{A-7}$$

We take the frequency ω to be sufficiently low that the term containing the displacement current $\partial\vec{D}/\partial t$ can be neglected. The constitutive relation between $\vec{H}$ and $\vec{B}$, in combination with Eq. 1, gives

$$\vec{H}(\vec{x},t) = \frac{1}{\mu}\vec{B}(\vec{x},t) = \frac{1}{\mu}\vec{\nabla} \times \vec{A}(\vec{x},t)\,. \tag{A-8}$$

Combining Eqs. A-6, A-7, and A-8, we obtain

$$\vec{\nabla} \times \vec{\nabla} \times \vec{A}(\vec{x},t) = \frac{4\pi\sigma\mu}{c}\,\left(\vec{\eta} - \frac{1}{c}\frac{\partial \vec{A}}{\partial t}\right). \tag{A-9}$$

A vector identity transforms the left-hand side of Eq. A-9, giving

$$\vec{\nabla}\left(\vec{\nabla} \cdot \vec{A}\right) - \nabla^2\vec{A} = \frac{4\pi\sigma\mu}{c}\,\left(\vec{\eta} - \frac{1}{c}\frac{\partial \vec{A}}{\partial t}\right). \tag{A-10}$$

In Coulomb gauge, where $\vec{\nabla} \cdot \vec{A} = 0$, Eq. A-10 reduces to

$$\nabla^2\vec{A}(\vec{x},t) = \frac{4\pi\sigma\mu}{c^2}\frac{\partial \vec{A}(\vec{x},t)}{\partial t} - \frac{4\pi\sigma\mu}{c}\vec{\eta}(\vec{x},t)\,. \tag{A-11}$$

Specializing to sinusoidal time dependence,

$$\vec{A}(\vec{x},t) = \vec{A}(\vec{x})\,e^{i\omega t} \tag{A-12}$$

$$\vec{\eta}(\vec{x},t) = \eta\,\hat{s}(\vec{x})\,e^{i\omega t}\,, \tag{A-13}$$

we reinterpret η and $\vec{A}(\vec{x})$ as complex (phasor) quantities. In terms of these phasors, Eq. A-11 becomes

$$\nabla^2\vec{A}(\vec{x}) - i\frac{4\pi\sigma\mu\omega}{c^2}\vec{A}(\vec{x}) = -\frac{4\pi\sigma\mu}{c}\eta\,\hat{s}(\vec{x})\,, \tag{A-14}$$

or, in SI units,

$$\nabla^2\vec{A}(\vec{x}) - i\omega\sigma\mu\vec{A}(\vec{x}) = -\sigma\mu\,\eta\,\hat{s}(\vec{x})\,. \tag{A-15}$$

Outside the wire, there is no current, so the right-hand side of Eq. A-11 vanishes, and the vector potential satisfies the Laplace equation:

$$\nabla^2\vec{A}(\vec{x}) = 0\,. \tag{A-16}$$

List of Symbols, Abbreviations, and Acronyms

AC	alternating current
ARL	Army Research Laboratory
DC	direct current
DEVCOM	US Army Combat Capabilities Development Command
DDM	domain decomposition method
MPM	mobile power meter
PDE	partial differential equation
THD	total harmonic distortion

1 (PDF)	DEFENSE TECHNICAL INFORMATION CTR DTIC OCA
1 (PDF)	DEVCOM ARL FCDD RLD DCI TECH LIB